Soft-Sensor based Operation of a Solid Oxide Fuel Cell System with Anode Exhaust Gas Recirculation

Schaefer, Felix[1,2,z]; Egger, Sebastian[1]; Steiner, Dietmar[1]; Carré, Maxime[1]; Eichel, Rüdiger-A.[2,3]

[1] Robert Bosch GmbH, Corporate Research, 71272 Renningen, Germany

[2] RWTH Aachen University, Institute of Physical Chemistry, 52074 Aachen, Germany

[3] Forschungszentrum Jülich GmbH, Institute of Energy and Climate Research, Fundamental Electrochemistry (IEK-9), 52425 Jülich, Germany

[z]Felix.Schaefer2@de.bosch.com

Abstract

A solid oxide fuel cell (SOFC) converts chemical energy of a fuel gas directly into electrical energy representing an auspicious technology for efficient electricity generation. A SOFC system with anode exhaust gas recirculation (AEGR) enables net electrical DC-efficiency of up to 65%. For efficient and durable operation, it is of crucial importance to monitor relevant characteristic parameters and keep them within safe and durable operating limits. The oxygen-to-carbon-ratio and the fuel utilization are such characteristic parameters and have to be kept within stack- and reformer-specific limits. Their control is not straightforward due to the enhanced complexity of a SOFC system with AEGR and dependence on fluctuating natural gas (NG) quality. In this paper, a soft-sensor concept is presented to determine the *H/C*-ratio of NG as measure of its quality with high accuracy. It is composed of an energy balance by means of enthalpy flow rates and Gaussian process regression models for estimation of unknown amount of inert gas species x_{N_2}, x_{CO_2} in NG as well as the enthalpy error as a corrector term of the ideal energy balance.

1 Introduction

Progressive global warming and growth of worldwide energy demand are currently one of the major challenges. For the respective reduction of greenhouse gas emissions

primary energy consumption an enhanced use of renewable energies as well as replacement of conventional energy converters with high carbon footprint by technologies with higher efficiency is needed [1,2]. One of the major promising technologies in this regard is the fuel cell [2–4]. Fuel cells are efficient electrochemical devices for power generation, which convert chemical energy directly into electrical energy by oxidizing a fuel gas.

One of the most promising fuel cell technologies represents the high temperature solid oxide fuel cell (SOFC). It uses nonprecious metals as electrocatalyst material of the electrodes and an ion-conducting ceramic as electrolyte, which simplifies the cell construction and eliminates a complex electrolyte management in comparison to low-temperature fuel cell types [5]. The resource-efficient use of nonprecious and abundant metals as electrocatalyst leads to lower costs and the potential of internal reformation of natural gas (NG) within the cell, offers a great fuel flexibility and a reduced complexity for fuel pre-processing [2,5–7]. Moreover, SOFC technology is enabling a high energy utilization with a net electrical efficiency of up to 65% with regard to direct current (DC) as output, which is the same order of efficiencies reached by large power plants [5,6,8–11]. This can be enhanced to an overall efficiency of around 90% by operation a combined heat and power generator, where heat in the exhaust gas with temperatures around 200°C is also used [2,4,5,7,9–14].

When using NG as fuel, the system configuration with increased efficiency can be obtained by anode exhaust-gas recirculation (AEGR), where a part of the depleted anode exhaust gas is recirculated and mixed with fresh NG prior to entering the reformer [15]. This increases electrical efficiency and supplies steam for the reforming process [14,15]. Next to cost reduction, faster start-up time and dynamic operating conditions caused by a high share of renewable energies in the near future, improvement of durability and enhanced system efficiency are core topics to be adressed for the SOFC technology [5,9,16–21]. This includes robustness to variations in NG quality supplied to the SOFC system, which can result from fluctuating NG quality itself or the feed-in of synthetic hydrogen or methane produced by Power-to-X technologies.

Characteristic parameters such as fuel utilization or the oxygen-to-carbon-ratio to avoid fuel depletion or carbon formation, respectively, are essential for optimal operation in this regard. They have to be kept within safe and durable operating ranges in dependence of stack- and reformer-specific limits [22]. For high system efficiency, the parameters need to be kept as narrow as possible to the limiting values though. An overview on control concepts of the fuel utilization and the oxygen-to-carbon-ratio with regard to SOFC systems with AEGR is given in Schäfer et al. [23]. It shall be also mentioned that a novel control concept of these characteristic parameters based on oxygen sensors in the fuel gas of a SOFC system is proposed by Schäfer et al. [24], where still some dependency on fuel gas composition is given.

The definition of the system and stack specific fuel utilization (*FU*) as well as the oxygen-to-carbon-ratio Ψ at the reformer inlet can be seen in equation (1), (2) and (3). A common control is a feed-forward control, which is based on uncertain parameters recirculation ratio r, NG coefficients K_{e^-}, K_o and K_c as well as molar flow rate of NG $\dot{n}_{NG}$. The cell number n_{cell} and current i_{cell} are known or measured.

$$FU_{sys} = \frac{i_{cell} \cdot n_{cell}}{\dot{n}_{NG} \cdot K_{e^-} \cdot F} \tag{1}$$

$$FU_{sta} = \frac{i_{cell} \cdot n_{cell}}{\mathrm{F} \cdot \dot{\mathrm{n}}_{\mathrm{gas,an,in}} \cdot \mathrm{K}_{\mathrm{e^-,an,in}}} = \frac{(1 - r) \cdot FU_{sys}}{1 - r \cdot FU_{sys}} \tag{2}$$

$$\Psi = \left(\frac{r \cdot FU_{sys} \cdot K_{e^-}}{2} + K_O\right)\frac{1}{K_C} \tag{3}$$

The uncertain parameters cannot be measured directly by a sensor and rely on NG composition, which quality is changing over time and normally is not constantly tracked [1,25,26]. Figure 1 lists the fluctuation range of major gas species contained in NG for some locations in Europe taken from Hering [25]. The major species contained in NG is methane with a share of ~80-90%. Additional species in NG are ethane, carbon dioxide, propane, nitrogen and butane. Sulfur is not included in the list, because it is only present in a neglectable low range of some parts per million (ppm) and is not included as measured variable in the NG data. In some studies it is stated that a sulfur content above 10 or even 2 ppm is sufficient to start catalyst deactivation [26–28]. More related

information on sulfur tolerance and poisoning is given in the related literature [29–32]. For more detailed information on the variation of NG compositions and the related standardization, the reader is referred to the relevant literature [25,33–38].

Installing concentration measurement devices at the system inlet is a possible and easy way to determine NG quality. However, it comes along with in most cases not acceptable additional costs and increases the size of a SOFC system. Accurate concentration measurements imply also long measurement times, which is caused by extractive measuring procedures [18,39–42]. These methods are thus unsuited for commercial usage.

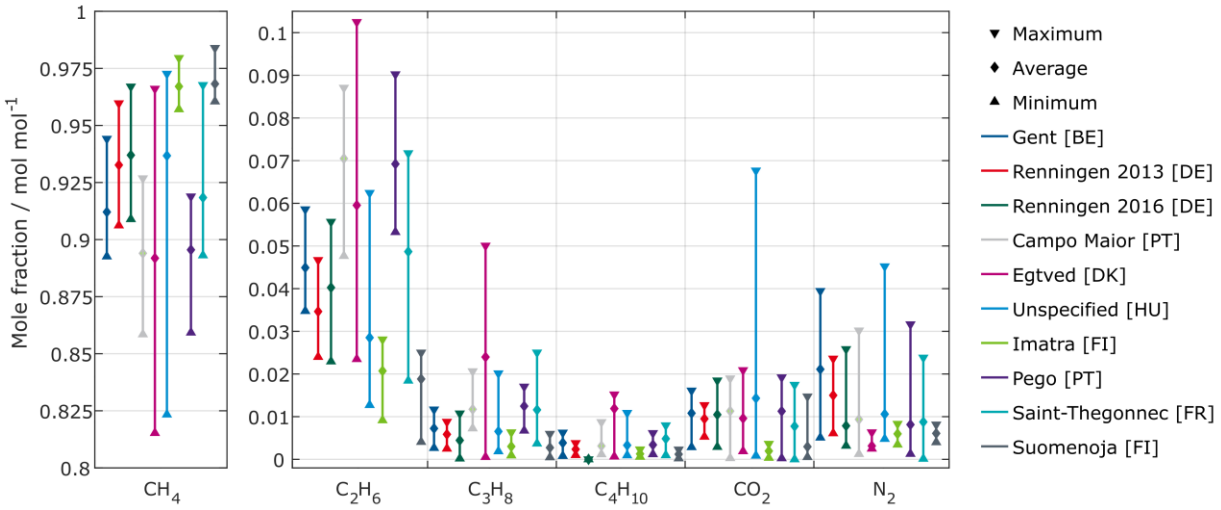

Figure 1: Composition range of NG in molar fraction for some locations in Europe (NG data is taken from Hering [25]).

The most common remedy represents a safety buffer of up to 10%-points on the characteristic parameters to ensure safe operation, which means a great amount of unused fuel gas in the stack and a loss in efficiency. A different method is thus needed to determine NG quality, where a respective concept is presented in this paper.

The remainder of this paper is structured as follows. Firstly, fundamentals regarding SOFC systems, gas coefficients and respective correlations as well as Gaussian process regression are outlined. Subsequently, the basic concept to use models of SOFC components (tail-gas burner, hotbox) as calorimeter is illustrated. The experimental procedure is followed by the results, which are divided into inert gas estimation,

estimation for enthalpy errors and the essential results for determination of *H/C*-ratio. A short summary and an outlook on further work is given in the last part of this paper.

2 Fundamentals

2.1 SOFC system

In the following s short introduction into the basics of a SOFC system is given. It shall be mentioned that further and more detailed information on SOFC systems have been given by the authors elsewhere [23,24].

A SOFC system includes the process steps gas treatment, electrochemical conversion and afterburning [5,9,12,26,43], where gas treatment consists of gas reforming and desulfurization and the electrochemical conversion happens in the stacks. It also contains some balance of plants components such as pumps, blowers, heat exchangers (HEX) and a tail-gas burner (TGB).

A detailed description of the SOFC system used for this study has been presented by Weeber [44] and in the work of Hering [25]. The SOFC system is intended for NG operation with a net electric power output of 10 kW and a net electric system efficiency of $\eta_{el,sys} \approx 60\%$. A simplified piping and instrumentation diagram is shown in figure 2. The SOFC system owns an AEGR, where depleted fuel gas at the anode outlet is partly recirculated with a blower and mixed with fresh NG. The recirculation ratio r is defined as the ratio of recirculated to total molar flow at the anode outlet and has two purposes [1,15,45]. For the avoidance of fuel depletion, a SOFC stack is limited mostly to a FU_{sta} in the range of 60 – 80% [1,21,43,46–49]. Recirculation of parts of the unused fuel leads thus to a higher utilization on system level and overall efficiency. Second, water vapor is in general needed for steam reforming. By recirculation of anode exhaust gas the water vapor is supplied without an external device or evaporator [50]. It has to be considered though that a too high recirculation rate leads to a dilution of the fuel gas. This essentially result in a drop of Nernst voltage of the SOFC cells and in the end to a lower power output [11,49,51].

Sulfur contained in NG is removed by an integrated desulfurization unit prior to the reformer [43,50]. NG contains long-chain hydrocarbons. These hydrocarbons need to be

cracked in a reforming process by means of of water vapor or oxygen. Overall aim of the reforming process is the supply a hydrogen-rich gas known as reformate to the SOFC moduule for the electrochemical conversion [5,11,26,52]. The SOFC module itself comprises one or more SOFC stacks with multiple cells. The reformate essentially takes part in an electrochemical conversion at the anode with oxygen anions [43,52].

Anode exhaust gas, which is not recirculated, and the oxygen depleted cathode exhaust air are supplied to the TGB. In the TGB a complete combustion has to be accomplished [43]. The heat in the exhaust gas is used internally of the SOFC system to preheat the air and NG. The hot components, being the SOFC module, TGB, reformer and heat exchangers, are assembled together in a common enclosure, named hotbox, to reduce heat losses.

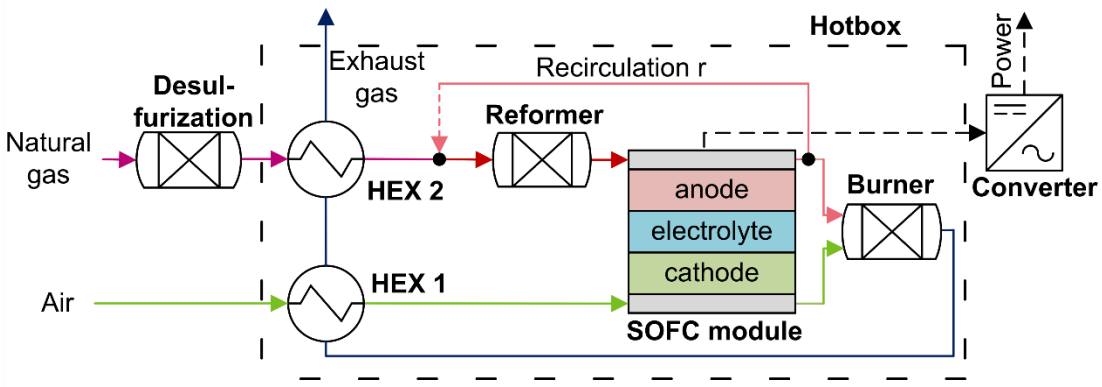

Figure 2: Basic structure of SOFC system by Bosch [25].

The SOFC itself is based on the planar metal supported cell (MSC) technology by Ceres[1] allowing stack operating temperatures of 500-600°C. The cells are composed of gadolinia-doped ceria (CGO) as electrolyte material, Lanthanum Perovskite for the cathode, Ceria-Nickel-Cermets as anode material as well as a laser drilled substrate made of ferritic stainless-steel foil [48]. The cells are assembled to 5 kW stacks, offering a FU_{sta} of up to 75%, an internal conversion of hydrocarbons such as CH_4 of up to 100% and an electrical efficiency $\eta_{el,FC}$ of > 63% based on the lower heating value of CH_4 [48].

[1] For more detailed information about the MSC technology by Ceres the reader is referred to the respective literature, such as [48,53].

SOFC system control is divided into a control for the air-supply and control for the supply of fuel gas. The supplied air is used to cool the SOFC module, which results in an air utilization *AU* << 100%. The air supply is controlled via a closed loop control to meet inlet and outlet temperature of the SOFC module. The fuel gas supply is based on a feedforward control of the NG flow rate and the recirculation flow rate r, as shown in equation (4) and (5) [15,25]. Therein Ψ and FU_{sta} need to be defined. NG composition needs to be known to calculate the respective gas coefficients K_C, K_O and K_{e^-}.

$$\dot{n}_{rec} = \dot{n}_{NG} \frac{(\Psi \cdot K_C - K_O)(1 + 2 \cdot K_C - K_O)}{FU_{sta}\left(\left(0.5 \cdot K_{e^-} - (\Psi \cdot K_C - K_O)\right)\right)} \tag{4}$$

$$\dot{n}_{NG} = \frac{i_{cell} \cdot n_{cell}}{F} \cdot \frac{1}{FU_{sta} \cdot K_{e^-} + 2(\Psi \cdot K_C - K_O)(1 - FU_{sta})} \tag{5}$$

According to equation (1) and (2) *FU* can be specified in a SOFC system with AEGR for the stack by means of the fuel flow rate at the anode inlet as FU_{sta} or for the overall system by means of the NG flow rate at the system inlet as FU_{sys} [1,7,11,15,17,25,39,45]. Without recirculation (r = 0) both definitions are equal, as it is stated in equation (2), where FU_{sys} and FU_{sta} are related via the recirculation-ratio r [11,15,39,45].

2.2 Gas coefficients and correlations

Gas coefficients are used to describe NG composition. These are the gas coefficients for carbon, oxygen, hydrogen and nitrogen as well as an electron gas coefficient in mol per mol. Since each NG type owns its proper coefficients, e.g. pure CH_4 has K_{e^-}= 8, the coefficients are used to classify gas mixtures. Two NG compositions with identical gas coefficients lead to identical behavior of the SOFC system [25]. The gas coefficients according to equation (6) to (9) for carbon, oxygen, hydrogen and nitrogen are calculated on the basis of the individual concentrations $x_{NG,i}$ and the corresponding number of atoms N_i contained in the respective molecule as weighting factor [25]. Each coefficient thus defines the number of atoms of a particular element (C,O,H,N) [25]. The electron gas coefficient according to equation (10) describes the amount of potentially releasable electrons in a complete electrochemical conversion in dependence of the number of electrons $N_{e^-,i}$ for each gas species i [11,25].

$$K_C = \sum_i x_{NG,i} \cdot N_{C,i} = x_{NG,CH_4} + 2x_{NG,C_2H_6} + 3x_{NG,C_3H_8} + 4x_{NG,C_4H_{10}} + x_{NG,CO_2} \quad (6)$$

$$K_O = \sum_i x_{NG,i} \cdot N_{O,i} = 2x_{NG,CO_2} \quad (7)$$

$$K_H = \sum_i x_{NG,i} \cdot N_{H,i} = 4x_{NG,CH_4} + 6x_{NG,C_2H_6} + 8x_{NG,C_3H_8} + 10x_{NG,C_4H_{10}} \quad (8)$$

$$K_N = \sum_i x_{NG,i} \cdot N_{N,i} = 2x_{NG,N_2} \quad (9)$$

$$K_{e^-} = \sum_i x_{NG,i} \cdot N_{e^-,i} = 8x_{NG,CH_4} + 14x_{NG,C_2H_6} + 20x_{NG,C_3H_8} + 26x_{NG,C_4H_{10}} + 2x_{NG,H_2} \quad (10)$$

An important parameter to describe NG composition is the ratio of H-atoms to C-atoms (*H/C*). The *H/C*-ratio correlates to K_{e^-}, K_C, K_H as well as other gas properties such as c_p (specific molar heat capacity of gas in J K^{-1} mol^{-1}) or specific enthalpy *h* (in J mol^{-1}).
New correlations for K_{e^-}, K_C, K_H are derived within this work with *H/C*-ratio as descriptive variable under the prerequisite of constant or known amount of inert gas species x_{N_2}, x_{CO_2}. These correlations for *H/C* ≤ 4 are shown in equation (11) to (14). The index “no” states that inert gas species are not considered for the respective *H/C*-ratio. The derivation of the correlations is given for the interested reader in appendix A.

$$K_{e^-} = \frac{2 \cdot \frac{H}{C}_{no} + 8}{\frac{H}{C}_{no} - 2} \cdot (1 - x_{N_2} - x_{CO_2}) \quad (11)$$

$$K_C = \frac{2}{\frac{H}{C}_{no} - 2} \cdot \left(1 - x_{N_2} - x_{CO_2}\right) + x_{CO_2} \quad (12)$$

$$K_H = \frac{2 \cdot \frac{H}{C}_{no}}{\frac{H}{C}_{no} - 2} \cdot (1 - x_{N_2} - x_{CO_2}) \quad (13)$$

$$\frac{H}{C}_{no} = \frac{2\frac{H}{C} \cdot (1 - a)}{2 - a \cdot \frac{H}{C}} \quad , \quad a = \frac{x_{CO2}}{1 - x_{N_2} - x_{CO_2}} \quad (14)$$

The relationship between *H/C*-ratio and K_{e^-}, K_C, K_H for *H/C* > 4 is specified using regressions. NG data for *H/C* > 4 are based on the limit gas G222 [54] and some arbitrary gas mixtures of CH_4 and H_2 up to a *H/C*-ratio of 12. Good correlations are defined without considering inert gas species initially ("no") and a subsequent respective conversion as shown in equation (15) to (17). The regressions are done with the curve fitting toolbox in Matlab [55]. The respective R-squared values as a measure for goodness-of-fit are for all regressions higher than 0.99 stating a high accuracy.

$$K_{e^-} = \left(173.3e^{-1.058\cdot\frac{H}{C}_{no}} + 7.338e^{-0.07295\cdot\frac{H}{C}_{no}}\right)\cdot\left(1 - x_{N_2} - x_{CO_2}\right) \tag{15}$$

$$K_C = \left(8.19e^{-1.183\cdot\frac{H}{C}_{no}} + 1.271e^{-0.1629\cdot\frac{H}{C}_{no}}\right)\cdot\left(1 - x_{N_2} - x_{CO_2}\right) + x_{CO_2} \tag{16}$$

$$K_H = \left(52.58e^{-1.016\cdot\frac{H}{C}_{no}} + 3.552e^{-0.03437\cdot\frac{H}{C}_{no}}\right)\cdot\left(1 - x_{N_2} - x_{CO_2}\right) \tag{17}$$

Heat capacity c_p and enthalpy *h* for NG are calculated based on a reference NG temperature by regression functions in equation (18) and (19) for *H/C* ≤ 4 and in equation (20) and (21) for *H/C* > 4 without considering inert species being part of NG composition. NG data for some locations in Europe is taken for *H/C* ≤ 4 from the work of Hering [25]. Inert gas species are taken into account by a respective conversion as shown in equation (22) to (23), where single c_p and h values are calculated based on NASA polynoms [56].

$$c_{p,no} = 8.944\left(\frac{H}{C}_{no}\right)^3 - 93.22\left(\frac{H}{C}_{no}\right)^2 + 308.1\frac{H}{C}_{no} - 274.3 \tag{18}$$

$$h_{no} = -1.283\cdot10^5\cdot e^{-0.1446\frac{H}{C}_{no}} - 6.42\cdot10^{-8}\cdot e^{5.933\frac{H}{C}_{no}} \tag{19}$$

$$c_{p,no} = 79.29e^{-0.6982\frac{H}{C}_{no}} + 33.34e^{-0.006864\frac{H}{C}_{no}} \quad (20)$$

$$h_{no} = -9.359 \cdot 10^5 \cdot e^{-0.819\frac{H}{C}_{no}} - 6.219 \cdot 10^4 \cdot e^{-0.1277\frac{H}{C}_{no}} \quad (21)$$

$$c_p = c_{p,no} \cdot (1 - x_{N_2} - x_{CO_2}) + c_{p,CO_2} \cdot x_{CO_2} + c_{p,N_2} \cdot x_{N_2} \quad (22)$$

$$h_{NG} = h_{no} \cdot (1 - x_{N_2} - x_{CO_2}) + h_{CO_2} \cdot x_{CO_2} + h_{N_2} \cdot x_{N_2} \quad (23)$$

A smooth transition between *H/C* ≤ 4 and *H/C* > 4 by equation (24) is used to ensure a continuous calculation of a variable needed for a stable solving process, where the function for *H/C* ≤ 4 is multiplied with $C_{transition}$ and the function for *H/C* > 4 is multiplied with (1-$C_{transition}$).

$$C_{transition} = 0.5 \cdot \left[1 + \tanh\left(-\frac{2\pi\left(\frac{H}{C} - 4\right)}{0.001}\right)\right] \quad (24)$$

3 Soft-sensor models of SOFC components

3.1 Basic concept

The soft-sensor concept proposed within this work represents a hybrid model combining physic-based and data-based model approaches, which is implemented with the open-software tool Python and the toolbox scikit-learn [57,58]. The basic idea is to model a component of a SOFC system with a simple energy balance as physic-based model by means of enthalpy flow rates in dependence of solely one unknown variable and enhance it with a data-based model. Input variables are measured variables such as volume flow rates, temperatures, stack current and voltage. The energy balance is solved by a numerical procedure determining the unknown variable. The model concept is based on the following assumptions:

- Presence of a stationary operating point
- Applicability of the ideal gas law
- Gas-tightness of the whole SOFC-system
- Complete combustion of fuel in TGB

The high-level approach of this concept is based on coupled mechanisms and dependencies within a SOFC system. Assuming constant manipulated variables (e.g. recirculation ratio, flow rate of NG, stack current) in a SOFC system, a change in NG compositions essentially results in a change of temperature at some location. As an example, change of NG composition to a lower heating value leads to a higher FU_{sta}. This in turn results in a lower amount of unconverted fuel gas at the TGB inlet, leading to a lower TGB outlet temperature. The correlation between NG composition and temperatures is essentially used to conclude about NG composition.

An energy balance is done at a component, which is not included in or encompasses the recirculation loop. As figure 2 shows, this holds true for the TGB, heat exchangers HEX 1, 2 or the hotbox. The remaining unknown is the *H/C*-ratio of NG. All other variables are measured or calculated quantities. This implies the prerequisite of constant or known amount of inert NG species x_{N_2}, x_{CO_2}. HEX 1 and 2 show only a small dependency on the *H/C*-ratio due to the sole heat exchange without fuel gas conversion. Better suited in this regard are the TGB and the hotbox being treated in this study.

Modelling a component with an ideal energy balance is always associated with some error in comparison to reality. It is stated as enthalpy error and includes measurement errors of variables, which enter the energy balance such as temperatures, as well as heat losses of the component. The operating point dependent enthalpy error of the component is modelled in advance with a Gaussian process (GP) regression model. GP modelling is a supervised machine-learning algorithm based on known training data for model generation, where some basic remarks on GP modelling is given in appendix B for the interested reader.

The GP regression model is used for correction of the ideal energy balance to achieve a good fit with the component's real behavior. Modelling of the enthalpy error is done by supplying a fuel gas with known composition such as CH_4 or by supplying NG in

conjunction with a high precision gas analyzer (e.g. gas chromatograph). Based on Dubourg et al. [59], the kernel for all the Gaussian process regression models used within this work is the product of a constant kernel and an RBF kernel. Multiplying the RBF by a constant kernel represents a scaling of the RBF kernel, which leads to a significant improvement in the accuracy of the enthalpy error estimation in terms of mean absolute error (MAE) with respect to validation data (see below).

The concept of the hybrid model can thus be generalized as stated in equation (25). Therein $\dot{H}_i$ is the enthalpy flux i coming or leaving a component, Var_{meas} and Var_{cal} describe measured and calculated variables used in the energy balance. It shall be noted that the enthalpy error term $\dot{H}_{error}$ comprises both the physical present heat loss of the specific component as well as the error of the ideal energy balance since it cannot be differentiated.

$$\sum_i \dot{H}_i \left(\frac{H}{C}; Var_{meas}; Var_{cal}\right) + \dot{H}_{error}(GP; Var_{meas}; Var_{cal}) = 0 \tag{25}$$

Based on the *H/C*-ratio the gas coefficient K_{e^-} is calculated by means of the correlation shown above. Subsequently FU_{sys} can be calculated by equation (1) and FU_{sta} can be calculated by equation (2) for known recirculation ratio. The method also allows to calculate the heat capacity c_p or density of NG. Using NG heat capacity, it is possible to correct the NG flow measured with a thermal flowmeter. Using NG density, the density at a recirculation blower can be determined to enhance recirculation ratio calculation.

3.2 Tailgasburner

The *H/C*-ratio in the TGB exhaust gas is calculated by performing an energy balance at its boundaries. Assuming a gas-tight system, the *H/C*-ratio in the TGB exhaust gas is equal to the *H/C*-ratio in the NG. The general energy balance is given in equation (26) and visualized in figure 3 (a) in dependence of the enthalpy fluxes entering and leaving the TGB. It is composed of the air and anode offgas (ao) entering (in) the TGB, offgas (og) leaving the TGB and the enthalpy error to adjust the ideal energy balance to the real behavior of the TGB.

$$\dot{H}_{air,TGB,in} + \dot{H}_{ao,TGB,in} - \dot{H}_{og,TGB,out} - \dot{H}_{error,TGB}(GP; Var_{meas}; Var_{cal}) = 0 \quad (26)$$

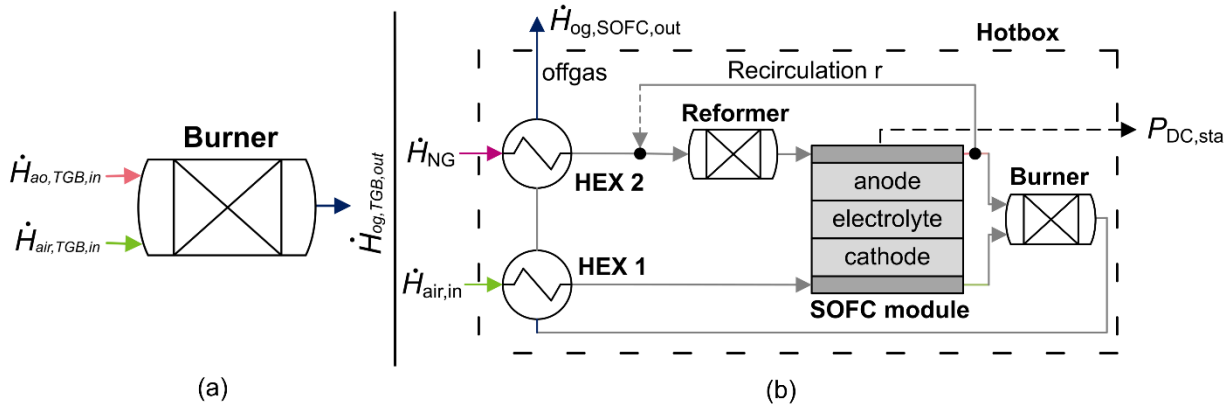

Figure 3: Visualization of enthalpy balance at the boundaries of the TGB (a) and at the boundaries of the hotbox.

The enthalpy flux of anode offgas entering the TGB $\dot{H}_{ao,TGB,in}$ is calculated according to equation (27) in dependence of the respective molar flow rate $\dot{n}_{ao,TGB,in}$ and specific enthalpy $h_{ao,TGB,in}$. The specific enthalpy is calculated as sum of the enthalpies for the individual gas species such as H_2, H_2O, CO_2, CO, CH_4 and N_2, which are weighted with its concentrations as shown in equation (28). Specific individual enthalpies $h_{i,ao,TGB,in}$ are calculated based on NASA polynoms [56] in dependence of gas temperature, which is a measured quantity. The concentrations of the individual gas species are calculated under the assumption of thermodynamic equilibrium by means of minimization of Gibbs energy for constant pressure and temperature [60–62]. Within this work, the open-source software Cantera [62] in conjunction with the database USC-Mech II [63] is used for calculation of chemical equilibrium, based on theory by Smith and Missen [64–66]. Input variables are the atomic quantity of oxygen, carbon, hydrogen and nitrogen with respect to carbon, yielding in the *O/C*-ratio, 1, *H/C*-ratio and *N/C*-ratio. *H/C*-ratio is the quantity of interest, which is supposed to be calculated. *N/C*-ratio is a constant quantity for stationary operating conditions. *N/C*-ratio can thus be calculated by the ratio of $K_N = 2x_{N_2}$ and K_C in NG, where the latter is expressed as function of the *H/C*-ratio as shown above. The *O/C*-

ratio downstream of the stack is defined in equation (29) in dependence of known (n_{cell}, V_{norm}, x_{CO_2}, F), measured (i_{cell}, $\dot{V}_{NG}$) or calculated quantities (K_C).

$$\dot{H}_{ao,TGB,in} = \dot{n}_{ao,TGB,in} \cdot h_{ao,TGB,in}\left(t_{ao,TGB,in}\,; x_{i,ao,TGB,in}\right) \tag{27}$$

$$h_{ao,TGB,in}\left(t_{ao,TGB,in}\,; x_{i,ao,TGB,in}\right) = \sum_i h_{i,ao,TGB,in} \cdot x_{i,ao,TGB,in} \tag{28}$$

$$\frac{O}{C}_{ao,TGB,in} = \frac{\Delta\dot{n}_{O,sta}}{\dot{n}_{NG} \cdot K_C} + \frac{2x_{CO_2}}{K_C} = \frac{\frac{i_{cell} \cdot n_{cell} \cdot V_{norm}}{2F} + 2x_{CO_2} \cdot \dot{V}_{NG}}{K_C \cdot \dot{V}_{NG}} \tag{29}$$

Assuming no gas leakage in the SOFC system, the molar flow rate of carbon atoms is constant and is used to describe the molar flow rate of fuel gas entering the TGB by equation (30). The gas composition at TGB inlet is calculated as mentioned above.

$$\dot{n}_{ao,TGB,in} = \frac{\dot{n}_{NG} \cdot K_C}{x_{CH_4,ao,TGB,in} + x_{CO,ao,TGB,in} + x_{CO_2,ao,TGB,in}} \tag{30}$$

The enthalpy flux of air $\dot{H}_{air,TGB,in}$ is calculated by equation (31). The specific enthalpy for nitrogen and oxygen is calculated by means of NASA polynoms [56] in dependence of the respective temperature. The cathode outlet oxygen molar flow rate is calculated according to equation (32) in dependence of the oxygen amount entering the SOFC system and the cell current. Since N_2 is an inert species, its amount stays constant and its molar flow rate is calculated by equation (33) in dependence of the oxygen amount in ambient air, which is typically around 21%.

$$\dot{H}_{air,TGB,in} = \dot{n}_{N_2,air,TGB,in} \cdot h_{N_2,air,TGB,in} + \dot{n}_{O_2,air,TGB,in} \cdot h_{O_2,air,TGB,in} \tag{31}$$

$$\dot{n}_{O_2,air,TGB,in} = \dot{n}_{air,in} \cdot x_{O_2,in} - \frac{i_{cell} \cdot n_{cell}}{4F} \tag{32}$$

$$\dot{n}_{N_2,air,TGB,in} = \dot{n}_{air,in} \cdot \left(1 - x_{O_2,in}\right) \tag{33}$$

For a complete combustion in the TGB, the enthalpy flux of the offgas $\dot{H}_{og,TGB,out}$ is expressed by equation (34) to (38). The respective specific enthalpies are calculated by means of NASA polynoms [56].

$$\dot{H}_{og,TGB,out}\left(t_{og,TGB,out}\,;x_{i,og,TGB,out}\right)=\sum_{j=CO_2,H_2O,O_2,N_2}\dot{n}_{j,og,TGB,out}\cdot h_j\left(t_{og,TGB,out}\right) \quad (34)$$

$$\dot{n}_{CO_2,og,TGB,out}=\dot{n}_{NG}\cdot K_C \quad (35)$$

$$\dot{n}_{H_2O,og,TGB,out}=\dot{n}_{NG}\cdot K_C\cdot\frac{H}{C}\cdot\frac{1}{2} \quad (36)$$

$$\dot{n}_{O_2,og,TGB,out}=\dot{n}_{air,in}\cdot x_{O_2,in}-\dot{n}_{CO_2,og,TGB,out}+\dot{n}_{NG}\cdot x_{CO_2,NG}-\frac{1}{2}\dot{n}_{H_2O,og,TGB,out} \quad (37)$$

$$\dot{n}_{N_2,og,TGB,out}=\dot{n}_{air,in}\left(1-x_{O_2,in}\right)+x_{N_2,NG}\cdot\dot{n}_{NG} \quad (38)$$

The enthalpy error $\dot{H}_{error,TGB}$ is modeled with a GP regression model to achieve a good fit with the real TGB behavior, using available measurement data from the SOFC system at different operating points. It is modelled by some training data supplying CH_4 as fuel gas, which has a constant *H/C*-ratio of 4, and NG in conjunction with measurements by a high precision gas chromatograph system (Agilent 7890 [67]).

By inserting all the equations in the main equation (26) for the TGB energy balance, all input variables are measured or calculated values, except the *H/C*-ratio, which is the unknown of interest and is calculated using a numerical process.

3.3 Hotbox

The Hotbox is the second component used within this study as calorimeter to estimate *H/C*-ratio in the exhaust gas by performing an energy balance at its boundaries. Assuming a gas-tight system, it is equal to the *H/C*-ratio in the NG feed line.

The general energy balance is given in equation (39) and shown in figure 3 (b) in dependence of the enthalpy fluxes entering and leaving the hotbox. It is composed of the air and NG entering (in) the hotbox, offgas (og) leaving the hotbox, electric DC power of the stack and the enthalpy error.

$$\dot{H}_{air,in}+\dot{H}_{NG}-\dot{H}_{og,SOFC,out}-\dot{H}_{error}(GP;Var_{meas};Var_{cal})-P_{DC,sta}=0 \quad (39)$$

The electric DC power of the stack $P_{DC,sta}$ is calculated as product of the measured stack voltage and current. The enthalpy flux of NG $\dot{H}_{NG}$ is calculated according to equation (40) in dependence of the respective molar flow rate $\dot{n}_{NG}$ and specific enthalpy h_{NG}, where the latter is calculated by equation (23). The molar flow rate $\dot{n}_{NG}$ is defined by equation (41) in dependence of the volume flow rate and the molar volume of ideal gas. NG volume flow rate is controlled with a thermal mass flow meter calibrated with CH_4. The measured volume flow rate is thus adjusted by NG temperature as well as the specific heat capacity of CH_4 and NG, which is expressed as a function of the *H/C*-ratio as shown above.

$$\dot{H}_{NG} = \dot{n}_{NG} \cdot h_{NG} \tag{40}$$

$$\dot{n}_{NG} = \frac{\dot{V}_{NG}}{V_{norm}} \tag{41}$$

The enthalpy flux of air $\dot{H}_{air,in}$ entering the hotbox is calculated by equation (42). The specific enthalpy for nitrogen and oxygen is calculated by means of NASA polynoms [56]. The molar flow rate of O_2 and N_2 are calculated by equation (43) and (44) in dependence of the ambient oxygen amount and measured volume flow rate of air.

$$\dot{H}_{air,in} = \dot{n}_{N_2,air,in} \cdot h_{N_2,air,in} + \dot{n}_{O_2,air,in} \cdot h_{O_2,air,in} \tag{42}$$

$$\dot{n}_{O_2,air,in} = \frac{\dot{V}_{air,in}}{V_{norm}} \cdot x_{O_2,in} \tag{43}$$

$$\dot{n}_{N_2,air,in} = \frac{\dot{V}_{air,in}}{V_{norm}} \left(1 - x_{O_2,in}\right) \tag{44}$$

With the sole difference in gas mixture temperature, the enthalpy flux of the offgas $\dot{H}_{og,SOFC,out}$ is calculated by equation (45) analogously to the enthalpy flux of the TGB offgas in equation (34). After the complete conversion in the TGB, there is no further change in gas composition, but a change in temperature due to internal heat recovery in the SOFC system. The respective specific enthalpies are calculated by means of NASA polynoms [56] and the molar flow rates by equation (35) to (38).

$$\dot{H}_{og,SOFC,out}\left(t_{og,SOFC,out}\,;x_{i,og,TGB,out}\right) = \sum_{j=CO_2,H_2O,O_2,N_2} \dot{n}_{j,og,TGB,out}\cdot h_j\left(t_{og,SOFC,out}\right) \quad (45)$$

The enthalpy error $\dot{H}_{error}$ is modeled with a GP regression model, using available measurement data from the SOFC system supplying CH_4 and NG as fuel gas.

By inserting all equations in the main equation (39), all input variables are measured or calculated values, except the *H/C*-ratio, which is the unknown of interest and is calculated using a numerical process to solve the energy balance.

4 Experimental procedure and results

4.1 Experimental procedure

Real data of a SOFC system is required for the implementation of the concepts. It concerns the measured values of volume flow rates, temperatures, voltage and current of the stack. Data from a SOFC system as outlined in figure 2 is used. This includes SOFC system operation with real NG in Renningen, Germany, as well as operation with CH_4. The NG operation of the SOFC system was accompanied with an intensive analysis of the supplied NG with measurements by a high precision gas chromatograph system (Agilent 7890B [67]).

For the implementation of the presented models, constant and stationary operating conditions of the SOFC system are required. The operating conditions of the SOFC system are therefore reduced by transient state points. The variables for the verification of steady-state operating conditions are chosen in such a way that the influences of the thermal capacities of the main components (reformer, stack, afterburner, hotbox) are captured by respective temperatures and volume flow rates. A steady-state detection algorithm is used for preselection, which is based on the comparison of the variance of a measured variable with the corresponding variance limit of a reference signal. Data points are eliminated, which occur consecutively (within a 2h interval) or are almost identical and thus do not contribute to knowledge on system behavior. From 186 data points in total, 47 and 85 data points for operation with NG and CH_4 are finally available for training and

validation of the models. An overview and its division into training and validation data is listed in .

Table 1. The data points include combinations of values for FU_{sta} (55, 60, 65%) and four different cell currents (13.5, 16, 17, 22.2 A) as setpoints. For safety reasons to avoid coking, Ψ has been limited to a fixed value of 2.4 based on feed-forward control. Data is sorted into training and validation data in a way that ensures that a given combination of setpoints is included at least once in the training data.

Table 1: Overview of CH_4 and NG data and its division into training and validation data

Type of fuel gas	Total	Training	Validation	Training + Validation
CH_4	115	17	68	85
NG	71	18	29	47
Total (NG + CH_4)	186	35	97	132

4.2 Inert gas species estimation

The presented concepts are based on the assumption that the concentrations of CO_2 and N_2 are known or constant. The latter is not true for NG from the grid. Since it is aimed to determine the *H/C*-ratio without NG analysis, these variables can also not be assumed as known. Despite the small variation range of a few percentages, it is found that the exact concentration values have some influence on model performance and the calculation of the *H/C*-ratio. Its influence is thus not negligible and the assumption of constant values cannot be considered reasonable. Accordingly, a determination of these two quantities must be included in the soft-sensor concept.

It is done by estimation of the concentration values using GP regression models and available measurement data from the SOFC system. To determine the input variables of the GP regression models, Pearson's correlation coefficients are used to quantify a sufficient and meaningful correlation by limitation to values between 0.5 and 1 (perfect

correlation) as well as -0.5 to -1 (perfect inverse correlation) [68]. The Pearson correlation coefficient is a measure of the linear correlation between two features.

The input variables of the GP regression model for estimating CO_2 concentration are the volume flow rates of supplied NG and air to the SOFC system as well as its temperatures, inlet and outlet temperature of the reformer and the temperatures of the offgas after the TGB. Further variables are the outlet temperature of the fuel gas and the outlet temperature of air at an internal heat exchanger. The same parameters are used as input variables for N_2 estimation, except the reformer outlet temperature.

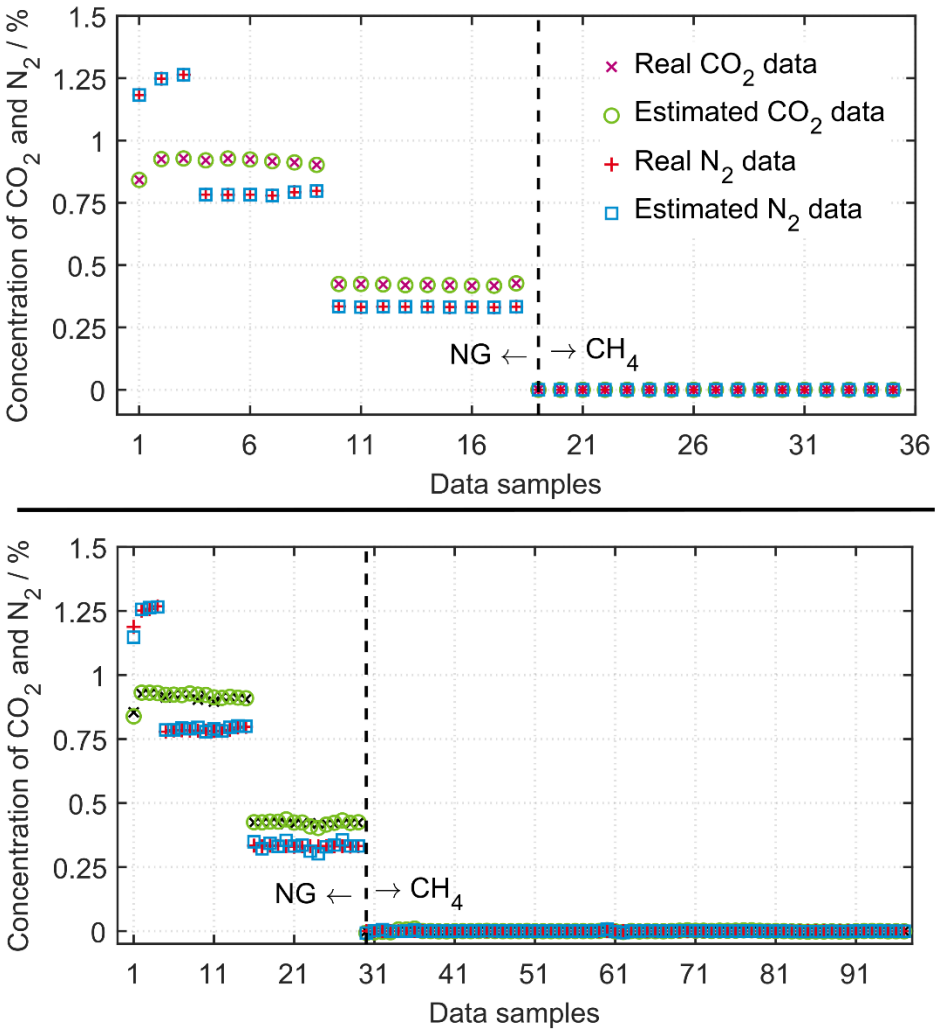

Figure 4: Estimation results for GP regression models for estimation of CO_2 and N_2 concentrations in NG and CH_4 based on training data (a) and based on validation data samples without CO_2 and N_2 as input variables.

The accuracy of the GP regression models with respect to training and validation data are shown in figure 4 (a) and figure 4 (b). A negligible deviation is achieved for the training data in figure 4 (a), which is attributed to its use for training of the GP regression models. A good accuracy of the overall estimation on validation data is shown in figure 4 (b). Small deviations in the estimation in figure 4 (b) are present for data point 1 and 24 for both CO_2 and N_2, where the latter is accompanied by some negligible low deviations for the neighboring data samples. Data point 1 and data point 24 are both operated with an

FU_{sta} of 65% and a cell current of 22.2 A, which are similar to other operating conditions used as data points within the study though. A respective influence of a unique operating point is therefore not present for data point 24, which means that the deviations cannot be attributed to it. At data point 1 the SOFC system has been operated with a slightly smaller recirculation ratio compared to the other data points, to which the deviations can accordingly be attributed.

The analysis with the Pearson correlation coefficients also showed a mutual interference of CO_2 and N_2. Its concentration is therefore added as mutual input variable for the GP regression models. Figure 5 (a) shows the respective results for estimation of CO_2 and N_2 concentrations on the relevant validation data.

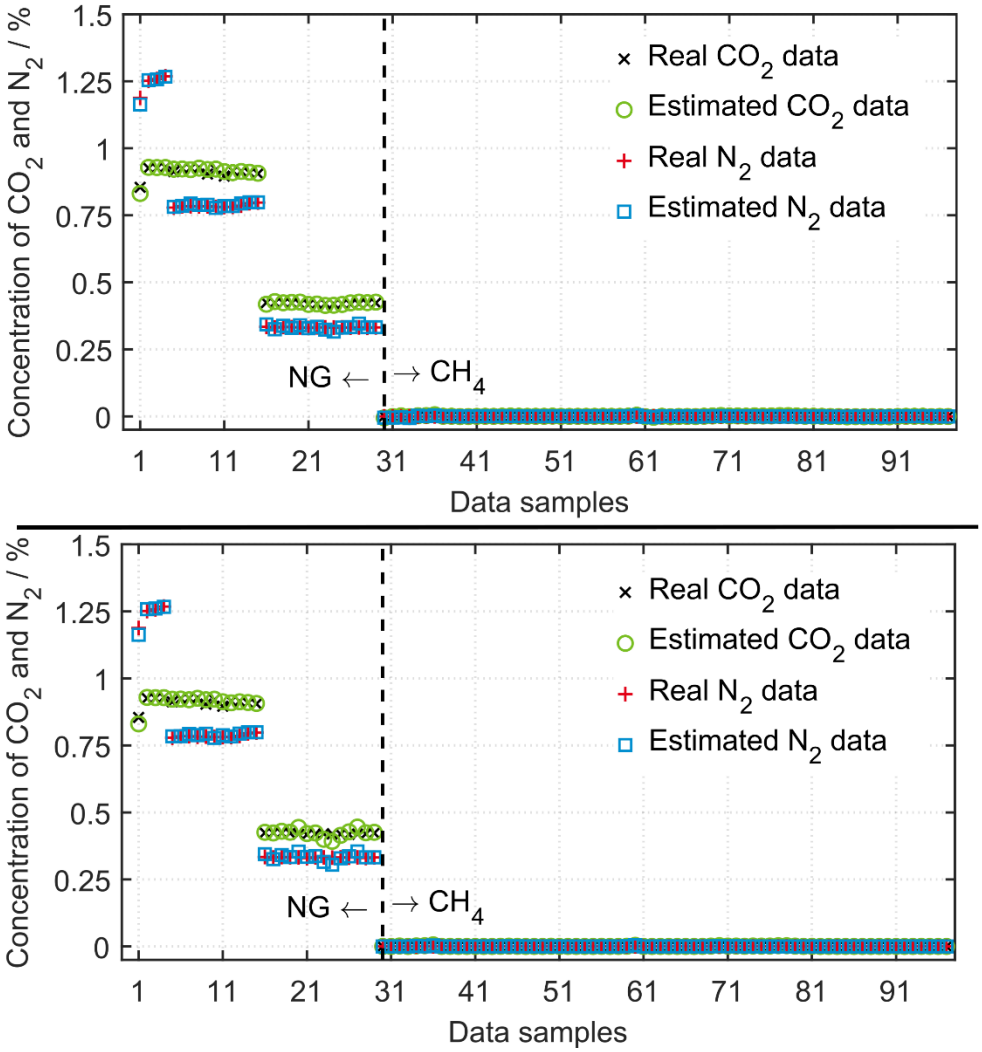

Figure 5: Estimation results for GP regression models for estimation of CO_2 and N_2 concentrations in NG and CH_4 based on validation data samples with real CO_2 and N_2 as mutual input variables (a) and final results of procedure implemented in the components models (b).

Figure 5 (a) states a higher accuracy of the CO_2 and N_2 estimation than the results presented in figure 4 (b) without CO_2 and N_2 as input variables. Small deviations in the estimation are still present for data point 1 for both CO_2 and N_2. The deviations of the estimation in data point 24 and its neighboring data points has been improved significantly

by the mutual integration. The mutual integration of inert gas species concentrations is therefore an improvement in the overall estimation quality.

Since no concentration value is available at the beginning of the calculation process for either CO_2 or N_2, the following procedure is applied. In a first step, the CO_2 fraction is estimated without N_2 as input variable as shown in Figure 4. In a second step, the N_2 fraction is estimated, where the estimated CO_2 concentration from the first step is included as input variable. In a third step, the CO_2 fraction is determined with the N_2 concentration of the second step as input variable. The N_2 fraction from the second step and the CO_2 fraction from the third step are then used in the soft-sensor models.

Figure 5 (b) shows the results of this procedure based on the validation data. Some small deviations in the estimation are again present for the data samples around data point 24 for both CO_2 and N_2. While being similar to the deviations shown in figure 4 for the estimation results without CO_2 and N_2 as mutual input variables, the deviations in figure 5 (b) are smaller in the mean. The GP regression models exhibit therefore a good overall estimation quality, which leads to a significant improvement compared to the assumption of constant concentrations of e.g. 0.5%.

4.3 Estimation results for enthalpy errors

The input variables of the GP regression model estimating the TGB enthalpy error are essentially variables used in the basic model. Explicitly, these are the cell current, the volume flow rates of supplied NG and air to the SOFC system, CO_2 and N_2 concentration, the temperatures at the inlet and outlet of the TGB as well as the temperature of the supplied NG. Based on a sensitivity analysis, it could be shown that stack voltage and the temperature of the offgas leaving the SOFC system has a positive influence on estimation quality and are included as input variables. For estimating the enthalpy error of the hotbox, input variables of the GP regression model are the electric DC power of the stack, the volume flow rates of supplied NG and air to the SOFC system. Further input variables are CO_2 and N_2 concentration, the offgas temperature at the outlet of the hotbox as well as the temperature of the supplied NG and air. A sensitivity analysis has also shown that the temperature of air before the stack inlet has a positive influence on estimation quality and is included as input variable.

The GP regression models exhibit an improved estimation quality when the *H/C*-ratio is used as input variable. The GP regression model then must be included in the iterative solution of the enthalpy balance to determine the *H/C*-ratio. This leads to a much more complex model and carries a high risk of instability problems in the computational process. Since it does not deteriorate seriously the estimation quality, the enthalpy error is modeled independently of the *H/C*-ratio to ensure a stable computational process.
Estimation results for the enthalpy errors of the TGB and the hotbox with respect to the training and validation data are given in figure 6 (a) and (b). While there are no or only negligible deviations for the estimates on the training data, there are small deviations for the estimates on the validation data. The most significant deviation of the estimation is shown by both the hotbox and the TGB at data point 1. This is explained by comparison to the training data. As mentioned above represents data point 1 of the validation data an operation condition that occurs only once in the entire data set for training and validation regarding a slightly reduced recirculation ratio. Since a comparable data point does not occur in the training data the GP regression model may not have the ability to predict this point perfectly. The quantitative lack of SOFC data sets in steady state based on NG as fuel gas is naturally leading to uncertainties and inaccuracies in an empirical model. A broader base of NG data with different compositions combined with a wide variation of operating parameters that also covers this or other deviant behavior is here desirable. Except from data point 1 the GP regression models show a very high estimation quality of the enthalpy errors though.

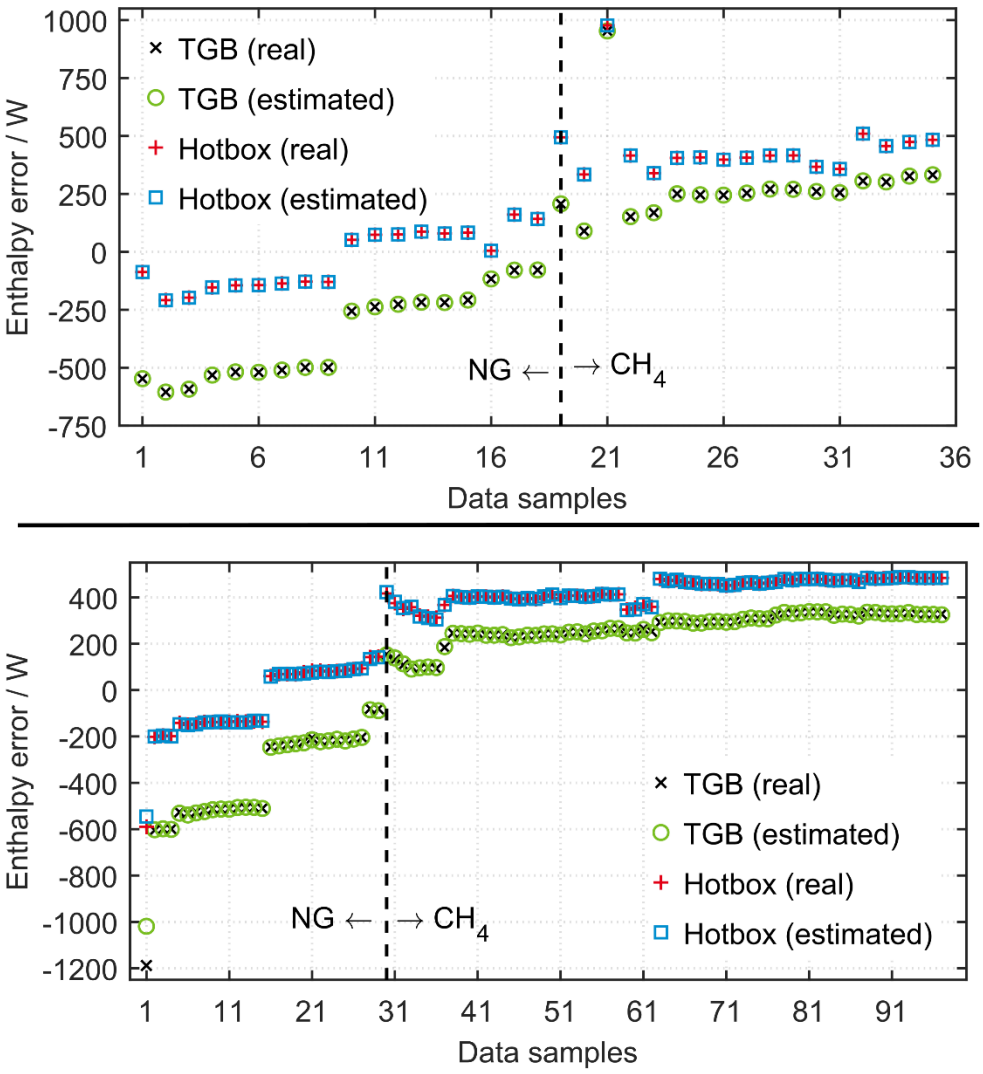

Figure 6: Estimation results for GP regression models for estimation of enthalpy errors for TGB and hotbox based on training data samples (a) and validation data samples (b).

4.4 Estimation results for *H/C*-ratio

Figure 7 shows the results for the estimation of the *H/C*-ratio on the training data for both the TGB and the hotbox. Figure 8 shows the results on the validation data for the TGB and the hotbox separately as well as its respective relative errors.

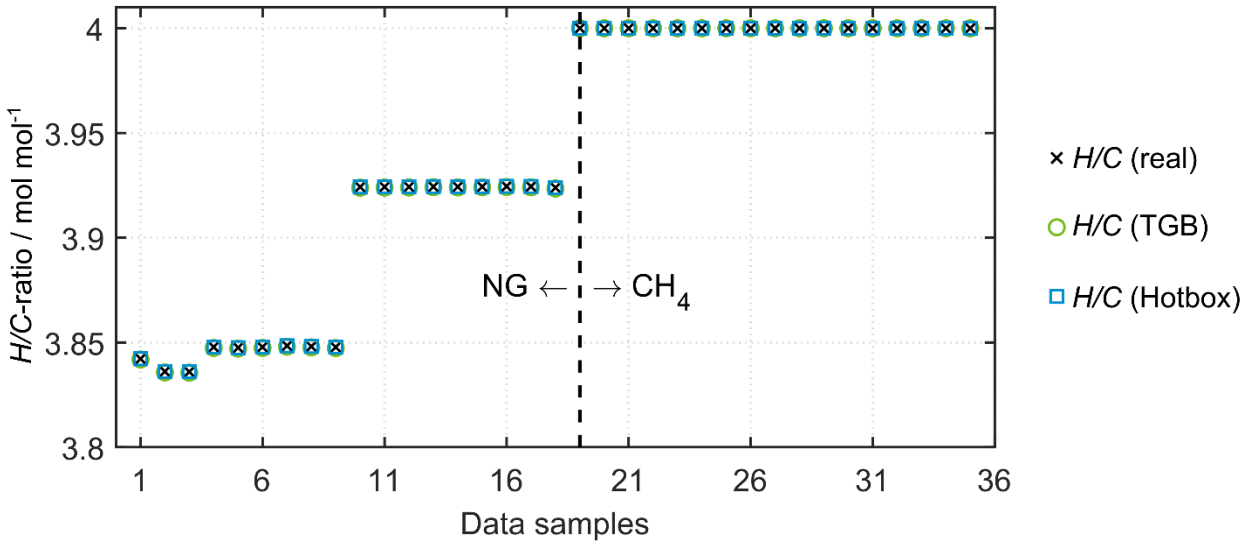

Figure 7: Results for determination of *H/C*-ratio with TGB and hotbox enthalpy model based on training data samples.

Figure 7 shows that there is a good agreement of the estimated *H/C*-ratio with the real values. With respect to the training data, an almost perfect agreement with a negligible deviation is achieved. This is attributed to the use of these data for the training of the Gaussian process models and a respective almost perfect estimation of CO_2, N_2 and the enthalpy errors. The results on the training data can thus not be distinguished between the two models (TGB, hotbox).

Differences are rather present on the validation data in figure 8 (a) and (b). The largest deviations occur at data point 1 as well as for the data samples around data point 24 with a relative error of about ±0.15% with respect to the real *H/C*-ratio, excluding data point 1 for the TGB model with a relative error of about -0.35%. While both CO_2 and N_2 estimates show slight inaccuracies at data point 1 and the data samples around 24, an inaccuracy of the estimate in the enthalpy errors is only present at data point 1.

At data point 1 the enthalpy error estimates deviate noticeably from the real value, which leads mainly to the maximum deviation of approximately -0.35% in the *H/C*-ratio for the TGB model and about -0.09% in the *H/C*-ratio for the hotbox model. For the data samples around data point 24 the N_2 and CO_2 estimates show a slight deviation from the real value, which leads to the deviations of ~ ±0.15% in the *H/C*-ratio. While no clear indication

about a respective share or influence on the *H/C*-ratio is given, it is expected that the determination of the *H/C*-ratio has a higher sensitivity to the CO_2 estimate and the influence of the N_2 estimate on the determination of the *H/C*-ratio is considered small. This is attributed to the fact that CO_2, in contrast to N_2, is not only included in the concentration shift of the other concentrations but also enters directly in the *H/C*-ratio as a variable.

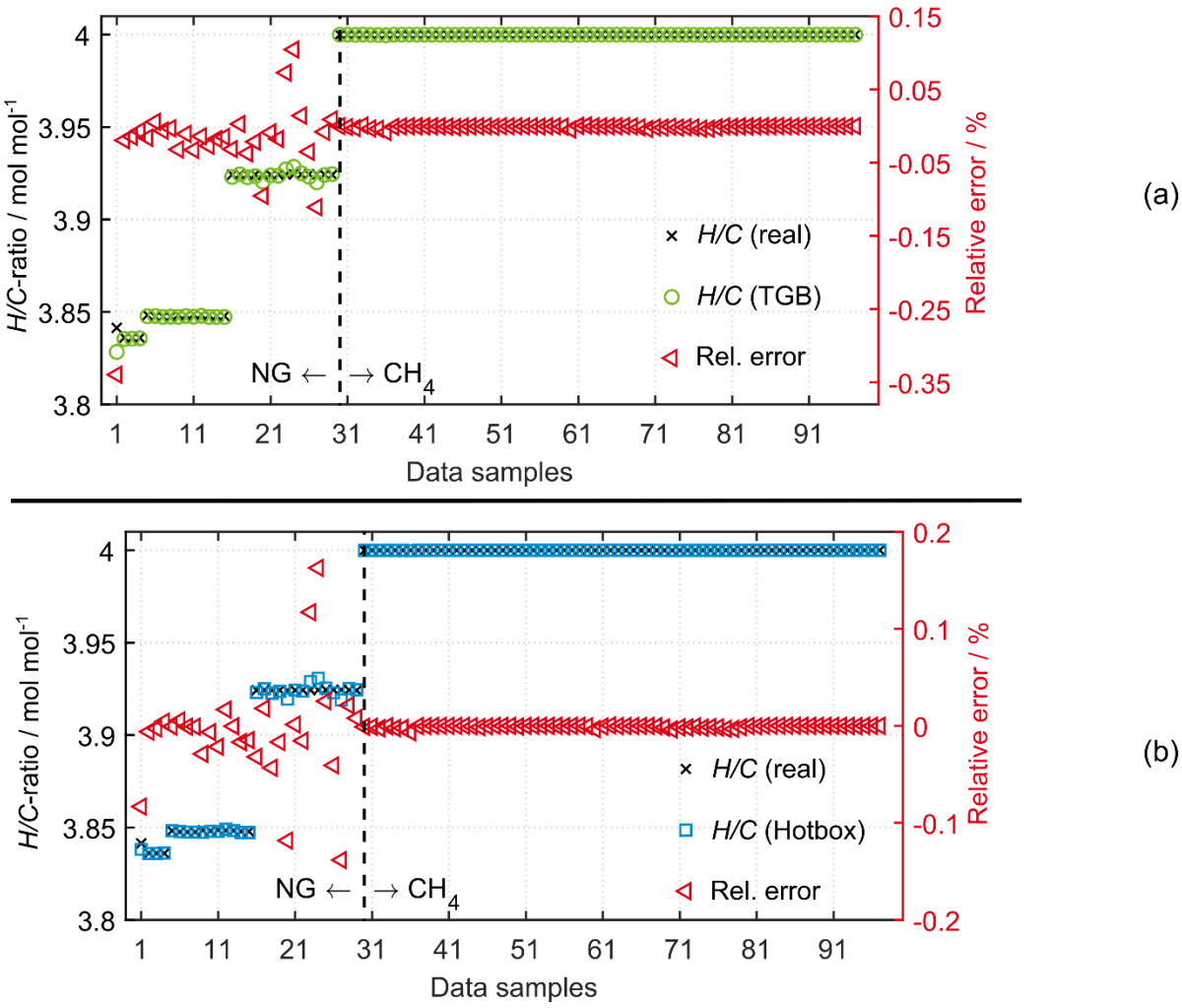

Figure 8: Results for determination of *H/C*-ratio with TGB enthalpy model (a) and hotbox enthalpy model (b) and their relative error based on validation data samples.

In comparison, both models (TGB, hotbox) show almost the same overall accuracy. While the TGB model shows the higher maximum inaccuracy at data point 1 with a maximum

deviation of only -0.35%, both models exhibit a good accuracy in average. This is reflected in a marginal difference of the MAE of 0.011% for the hotbox model and 0.022% for the TGB model on the validation data. Significant differences in accuracy are hard to notice. Only in data point 1, for the data samples around data point 24 and marginally in data point 36 are small differences present. The inaccuracies are at very low values though, which is why a high model quality is stated for both model approaches. Both models are thus suited and show a high potential for the determination of the *H/C*-ratio in NG.

5 Summary and conclusion

For safe and durable operation of a SOFC system it is of crucial importance to monitor the oxygen-to-carbon-ratio and fuel utilization and keep them within operating limits. Monitoring and control of these characteristic parameters is not trivial to both, the correlations within a SOFC system with AEGR and on fluctuating NG quality.

The authors present a soft-sensor concept to determine the *H/C*-ratio as measure of NG quality by a hybrid model approach. The hotbox and TGB of a SOFC system are modelled with an energy balance as physic-based model in dependency of the *H/C*-ratio as solely unknown. The enthalpy errors of the ideal energy balance are modeled with a GP regression model as data-based regression model. Other GP regression models are used to estimate the unknown amount of inert gas species x_{N_2}, x_{CO_2} in NG. Input variables are volume flow rates, temperatures, stack current and voltage. For stationary operation the energy balance is solved and the *H/C*-ratio is determined.

Both models show almost the same overall accuracy. While the TGB model shows the higher maximum inaccuracy at data point 1 with a maximum deviation of only -0.35%, both models exhibit a good accuracy in average. This is reflected in a marginal difference of the MAE of 0.011% for the hotbox model and 0.022% for the TGB model on the validation data. Significant differences in accuracy are hard to notice. The inaccuracies are at very low values, which is why a high model quality is stated for both model approaches showing a high potential for determination of the *H/C*-ratio.

Further studies, which need to be done subsequently include the following tasks:

- Derive a broader base of NG data with different compositions and variation of operating parameters.
- Extend offline tests to SOFC systems with different system layouts, analyze the differences and evaluate the potential to generalize the presented approach by a small calibration procedure to account for variations in system behavior.
- Performing of experimental tests directly on a real SOFC system for verification of the concept.

6 Nomenclature

Latin characters

Symbol	Meaning	Unit
a	Correction factor for *H/C*-ratio	-
C	Transition variable for *H/C*-ratio = 4	-
c_p	Specific molar heat capacity	J K^{-1} mol^{-1}
E	Expected value	-
f	Function	-
*f**	Estimated functional value with Gaussian process	-
F	Faraday-constant	C/mol
h	Specific enthalpy	J mol^{-1}
$\dot{H}_i$	Enthalpy flux	W
I	Current	A
i	Current density	A/cm^2
$k(x_i, x_j)$	Covariance function	-
K	Gas coefficients	-
l	Characteristic lengthscale	-
$m(x)$	Mean of Gaussian process	-
n	Number	-
$\dot{n}$	Molar flow rate of gas	Mol/s
P	Electrical power	W
r	Recirculation ratio	%
T	Temperature	°C
U	Voltage	V
V	Volume	l
$\dot{V}$	Volume flow rate	l/min
x	Concentration of gas spcies	%
x^*, x_i, x_j	Input variables for Gaussian process	-

Greek characters

Symbol	Meaning	Unit
$\Delta\dot{n}_O$	Difference in molar oxygen flow rate	mol s^{-1}
η	Efficiency	%
μ^*	Predicted variance in Gaussian process	-
σ_f^2	Signal variance	-
Ψ	Oxygen-to-carbon-ratio	mol mol^{-1}

Abbreviations

Abbreviation	Meaning
AC	Alternating current
AEGR	Anode exhaust-gas recirculation
AU	Air utilization
Cell	Single cell of a fuel cell
CH_4	Methane
C_2H_6	Ethane
C_3H_8	Propane
C_4H_{10}	Butane
CO	Carbon monoxide
CO_2	Carbon dioxide
DC	Direct Current
FC	Fuel cell
FU	Fuel utilization
GP	Gaussian Process
H_2	Hydrogen
H/C	Hydrogen-to-carbon-ratio
H_2O	Water

HEX	Heat exchangers
MAE	Mean absolute error
N_2	Nitrogen
NG	Natural gas
TGB	Tailgasburner
O_2	Oxygen
O/C	Oxygen-to-carbon-ratio
SOFC	Solid oxide fuel cell
Var	Variable

Subscripts

Subscript	Meaning
air	Supplied air to fuel cell
an	Anode
ao	Anode offgas
TGB	Tailgasburner
C	Carbon
cal	Calculated
cell	Cell of a fuel cell
DC	Direct current
e-	Electrons
El	Electrical
Error	Error
FC	Fuel cell
H	Hydrogen
i	Species i
in	Inlet
meas	Measured

N	Nitrogen
NG	Natural gas
No	No inert species considered
norm	Norm conditions
O	Oxygen
og	Offgas
out	Outlet
rec	recirculated
sta	Fuel cell stack
sys	Fuel cell system
Transition	Transition for *H/C*-ratio = 4

7 References

[1] S. Wahl, A.G. Segarra, P. Horstmann, M. Carré, W.G. Bessler, F. Lapicque, K.A. Friedrich, Journal of Power Sources 279 (2015) 656–666. https://doi.org/10.1016/j.jpowsour.2014.12.084.

[2] Y. Qin, G. Zhao, Q. Hua, L. Sun, S. Nag, Sustainability 11 (2019) 3290. https://doi.org/10.3390/su11123290.

[3] X. Wang, B. Huang, T. Chen, Journal of Process Control 17 (2007) 103–114. https://doi.org/10.1016/j.jprocont.2006.09.004.

[4] H. Meng, M. Han, Z. Sun, ECS Trans. 91 (2019) 81–90. https://doi.org/10.1149/09101.0081ecst.

[5] A. Choudhury, H. Chandra, A. Arora, Renewable and Sustainable Energy Reviews 20 (2013) 430–442. https://doi.org/10.1016/j.rser.2012.11.031.

[6] X. Wu, J. Jiang, H. Zhang, Z. Deng, X. Li, J. Li, in: 2018 Chinese Automation Congress (CAC), IEEE, 2018, pp. 1525–1530.

[7] M. Leung, G. Park, V. Radisavljevic-Gajic, in: 2013 9th Asian Control Conference (ASCC), IEEE, 2013, pp. 1–6.

[8] Darjat, Sulistyo, A. Triwiyatno, E. Julian, in: 2018 5th International Conference on Information Technology, Computer, and Electrical Engineering (ICITACEE), IEEE, 2018, pp. 234–239.

[9] M. Irshad, K. Siraj, R. Raza, A. Ali, P. Tiwari, B. Zhu, A. Rafique, A. Ali, M. Kaleem Ullah, A. Usman, Applied Sciences 6 (2016) 75. https://doi.org/10.3390/app6030075.

[10] Y.J. Park, G. Min, J. Hong, ECS Trans. 91 (2019) 2097–2104. https://doi.org/10.1149/09101.2097ecst.

[11] S. Wahl, Verfahrenstechnische Optimierung und Leistungsskalierung eines Festoxid-Brennstoffzellensystems mit Hilfe multiphysikalischer Modellierung und experimenteller Daten. Dissertation, 1. Auflage, 2015.

[12] P. Kurzweil, Brennstoffzellentechnik: Grundlagen, Materialien, Anwendungen, Gaserzeugung, 3. Edition, Springer Vieweg, Wiesbaden, 2016.

[13] ASUE, Brennstoffzellen für die Hausenergieversorgung, Berlin, 2018.

[14] Z. Lyu, M. Han, ECS Trans. 91 (2019) 1591–1600. https://doi.org/10.1149/09101.1591ecst.

[15] M. Carré, R. Brandenburger, W. Friede, F. Lapicque, U. Limbeck, P. da Silva, Journal of Power Sources 282 (2015) 498–510. https://doi.org/10.1016/j.jpowsour.2015.02.053.

[16] S.P. Shaikh, A. Muchtar, M.R. Somalu, Renewable and Sustainable Energy Reviews 51 (2015) 1–8. https://doi.org/10.1016/j.rser.2015.05.069.

[17] R.P. O'Hayre, S.-W. Cha, W.G. Colella, F.B. Prinz, Fuel cell fundamentals, Second edition, John Wiley & Sons Inc, Hoboken, New Jersey, 2009.

[18] B. Dolenc, D. Vrecko, D. Juricic, A. Pohjoranta, J. Kiviaho, C. Pianese, ECS Transactions 68 (2015) 2625–2636. https://doi.org/10.1149/06801.2625ecst.

[19] J. Mougin, B. Morel, A. Ploner, P. Caliandro, J. van Herle, P. Boškoski, B. Dolenc, M. Gallo, P. Polverino, A. Pohjoranta, A. Nieminen, S. Pofahl, J.P. Ouweltjes, S. Diethelm, A. Leonardi, F. Galiano, C. Tanzi, ECS Trans. 91 (2019) 731–743. https://doi.org/10.1149/09101.0731ecst.

[20] J.D. Sands, IOP Conf. Ser.: Mater. Sci. Eng. 639 (2019) 12018. https://doi.org/10.1088/1757-899X/639/1/012018.

[21] D. Vrečko, M. Nerat, D. Vrančić, G. Dolanc, B. Dolenc, B. Pregelj, F. Meyer, S.F. Au, R. Makkus, Đ. Juričić, International Journal of Hydrogen Energy 43 (2018) 6352–6363. https://doi.org/10.1016/j.ijhydene.2018.01.203.

[22] J. Chen, Y. Chen, H. Zhang, E3S Web Conf. 113 (2019) 2010. https://doi.org/10.1051/e3sconf/201911302010.

[23] F. Schäfer, S. Egger, D. Steiner, M. Carré, R.-A. Eichel, Journal of Power Sources 524 (2022) 231077. https://doi.org/10.1016/j.jpowsour.2022.231077.

[24] F. Schaefer, S. Egger, D. Steiner, R. Eichel, Fuel Cells (2021). https://doi.org/10.1002/fuce.202100034.

[25] M. Hering, Evaluation of the effects of varying fuel quality on solid oxide fuel cell systems. Dissertation, Clausthal, 2018.

[26] S.C. Singhal, K. Kendall (Eds.), High-temperature solid oxide fuel cells: Fundamentals, design and applications, Transferred to digital printing, Elsevier, Oxford, 2009.

[27] M. Carré, Modeling and control of a solid oxide fuel cell system with anode offgas recycle for residential combined heat and power generation. Dissertation, Der Andere Verl., Stuttgart, 2012.

[28] H. Chen, F. Wang, W. Wang, D. Chen, S.-D. Li, Z. Shao, Applied Energy 179 (2016) 765–777. https://doi.org/10.1016/j.apenergy.2016.07.028.

[29] M.T. Mehran, M.Z. Khan, S.-B. Lee, T.-H. Lim, S. Park, R.-H. Song, International Journal of Hydrogen Energy 43 (2018) 11202–11213. https://doi.org/10.1016/j.ijhydene.2018.04.200.

[30] A. Weber, S. Dierickx, N. Russner, E. Ivers-Tiffée, ECS Transactions 77 (2017) 141–147. https://doi.org/10.1149/07710.0141ecst.

[31] T. Hays, A.M. Hussain, Y.-L. Huang, D.W. McOwen, E.D. Wachsman, ACS Appl. Energy Mater. 1 (2018) 1559–1566. https://doi.org/10.1021/acsaem.7b00354.

[32] M. Riegraf, A. Zekri, V. Yurkiv, R. Costa, G. Schiller, K.A. Friedrich, ECS Transactions 77 (2017) 149–156. https://doi.org/10.1149/07710.0149ecst.

[33] G. Cerbe, B. Lendt (Eds.), Grundlagen der Gastechnik: Gasbeschaffung - Gasverteilung - Gasverwendung, 8. Edition, Hanser, München, 2017.

[34] H. Krause, A. Giese, H. Dörr, H.-J. Brückner, Hauptstudie zur Analyse der volkswirtschaftlichen Auswirkungen von Gasbeschaffenheitsschwankungen auf die Sektoren des Gasverbrauchs und deren Kompensation: Phase I: Hauptstudie Gasbeschaffenheit, Bonn, 2016.

[35] H. Krause, M. Werschy, S. Franke, A. Giese, J. Benthin, H. Dörr, Untersuchungen der Auswirkungen von Gasbeschaffenheitsänderungen auf industrielle und gewerbliche Anwendungen: Management Summary, Bonn, 2014.

[36] P. Nitschke-Kowsky, M. Angelo, W. Weßing, M. Vogt, Gasbeschaffenheit und ihre Schwankungen in E.ON-Verteilnetzen: Auswirkungen auf die Gasverwendung, Bonn, 2016.

[37] DIN Deutsches Institut für Normung e.V., Gasinfrastruktur – Beschaffenheit von Gas – Gruppe H, Beuth Verlag GmbH, Berlin.

[38] DVGW, Gasbeschaffenheit, Wirtschafts- und Verlagsgesellschaft Gas und Wasser mbH, Bonn 75.160.30.

[39] A. Gallet Segarra, Robust control of a solid oxide fuel cell for combined heat and power applications. Dissertation, Stuttgart, 2017.

[40] B. Dolenc, D. Vrečko, Đ. Juričić, A. Pohjoranta, C. Pianese, Journal of Power Sources 343 (2017) 246–253. https://doi.org/10.1016/j.jpowsour.2017.01.038.

[41] T. Das, R. Weisman, in: 2009 American Control Conference, IEEE, 2009, pp. 2767–2772.

[42] R.A. Potyrailo, J. Brewer, B. Scherer, V. Srivastava, M. Nayeri, C. Henderson, C. Collazo-Davila, M.A. Carpenter, N. Houlihan, V. Vulcano Rossi, A. Shapiro, ECS Trans. 91 (2019) 319–328. https://doi.org/10.1149/09101.0319ecst.

[43] K. Kendall, M. Kendall (Eds.), High-temperature solid oxide fuel cells for the 21st century: Fundamentals, design and applications, Academic Press is an imprint of Elsevier, London, 2016.

[44] K. Weeber, P. Horstmann, J. Miersch, in: Proceedings of the 13th European SOFC & SOE Forum 2018, Lucerne, Switzerland, 2018, pp. 12–14.

[45] L. Malafronte, B. Morel, A. Pohjoranta, Fuel Cells 18 (2018) 476–489. https://doi.org/10.1002/fuce.201700230.

[46] T. Das, R. Mukherjee, in: Volume 6: Energy Systems: Analysis, Thermodynamics and Sustainability, ASME, 2007, pp. 607–616.

[47] Q. Fang, L. Blum, R. Peters, M. Peksen, P. Batfalsky, D. Stolten, International Journal of Hydrogen Energy 40 (2015) 1128–1136. https://doi.org/10.1016/j.ijhydene.2014.11.094.

[48] R. Leah, A. Bone, E. Hammer, A. Selcuk, M. Rahman, A. Clare, S. Mukerjee, M. Selby, in: Proceedings of the 13th European SOFC & SOE Forum 2018, Lucerne, Switzerland, 2018, pp. 13–23.

[49] K. Huang, Journal of Power Sources 196 (2011) 2763–2767. https://doi.org/10.1016/j.jpowsour.2010.10.077.

[50] M. Boaro, A.A. Salvatore, Advances in Medium and High Temperature Solid Oxide Fuel Cell Technology, Springer International Publishing, Cham, 2017.

[51] T.-I. Tsai, L. Troskialina, A. Majewski, R. Steinberger-Wilckens, International Journal of Hydrogen Energy 41 (2016) 553–561. https://doi.org/10.1016/j.ijhydene.2015.10.025.

[52] H. Gorgun, M. Arcak, S. Varigonda, S. BORTOFF, International Journal of Hydrogen Energy 30 (2005) 447–457. https://doi.org/10.1016/j.ijhydene.2004.10.024.

[53] R.T. Leah, A. Bone, A. Selcuk, M. Rahman, A. Clare, M. Lankin, F. Felix, S. Mukerjee, M. Selby, ECS Trans. 91 (2019) 51–61. https://doi.org/10.1149/09101.0051ecst.

[54] G. Müller-Syring, M. Henel, Wasserstofftoleranz der Erdgasinfrastruktur inklusive aller assoziierten Anlagen, Bonn, 2014.

[55] MATLAB, 9.3.0.948333 (R2017b), The MathWorks Inc., Natick, Massachusetts, 2017.

[56] B.J. McBride, S. Gordon, M.A. Reno, Coefficients for calculating thermodynamic and transport properties of individual species, Cleveland, 1993.

[57] Lars Buitinck, Gilles Louppe, Mathieu Blondel, Fabian Pedregosa, Andreas Mueller, Olivier Grisel, Vlad Niculae, Peter Prettenhofer, Alexandre Gramfort, Jaques Grobler, Robert Layton, Jake VanderPlas, Arnaud Joly, Brian Holt, Gaël Varoquaux, in: ECML PKDD Workshop: Languages for Data Mining and Machine Learning, 2013, pp. 108–122.

[58] F. Pedregosa, G. Varoquaux, A. Gramfort, V. Michel, B. Thirion, O. Grisel, M. Blondel, P. Prettenhofer, R. Weiss, V. Dubourg, J. Vanderplas, A. Passos, D. Cournapeau, M. Brucher, M. Perrot, E. Duchesnay, Journal of Machine Learning Research 12 (2011) 2825–2830.

[59] V. Dubourg, J. Vanderplas, J. Metzen, Gaussian Processes regression: basic introductory example, 2021, https://scikit-learn.org/stable/auto_examples/gaussian_process/plot_gpr_noisy_targets.html#sphx-glr-auto-examples-gaussian-process-plot-gpr-noisy-targets-py.

[60] T. Bosch, Characterization of a novel radial reactor for a solid oxide fuel cell system with anode off-gas recirculation. Dissertation, Duisburg-Essen, 2018.

[61] D. Saebea, A. Arpornwichanop, Y. Patcharavorachot, International Journal of Hydrogen Energy (2020). https://doi.org/10.1016/j.ijhydene.2020.07.264.

[62] D.G. Goodwin, H.K. Moffat, R.L. Speth, Cantera: An Object-Oriented Software Toolkit For Chemical Kinetics, Thermodynamics, And Transport Processes. Version 2.4.0, Zenodo, 2017.

[63] H. Wang, X. You, A.V. Joshi, S.G. Davis, A. Laskin, F. Fokion Egolfopoulos, C.K. Law, USC Mech Version II: High-Temperature Combustion Reaction Model of H2/CO/C1-C4 Compounds, 2007, http://ignis.usc.edu/Mechanisms/USC-Mech%20II/USC_Mech%20II.htm.

[64] W.D. Seider, C.W. White, AIChE J. 31 (1985) 176. https://doi.org/10.1002/aic.690310127.

[65] W.R. Smith, Chemical reaction equilibrium analysis, Wiley, S.l., 1982.

[66] W.R. Smith, R.W. Missen, Chemical reaction equilibrium analysis: Theory and algorithms, Reprint ed., with corrections, Krieger, Malabar Fla., 1991.

[67] Agilent, Agilent 7890B Gas Chromatograph, Santa Clara, 2013.

[68] J. Cohen, Statistical power analysis for the behavioral sciences, 2nd ed., L. Erlbaum Associates, Hillsdale, N.J., 1988.

[69] F. Massa Gray, Gaussian process building models and their application in model predictive control. Dissertation, Stuttgart, 2017.

[70] H. Kracker, Modellierung und Kalibrierung von Computermodellen mit Anwendung auf einen Umformprozess. Dissertation, Technical University of Dortmund, Dortmund, 2011.

[71] W.W. Xing, F. Yu, P.K. Leung, X. Li, P. Wang, A.A. Shah, Journal of Power Sources 482 (2021) 228930. https://doi.org/10.1016/j.jpowsour.2020.228930.

[72] B. Dolenc, M. Stepancic, D. Juricic, J. Kocijan, D. Marra, C. Pianese, in: 2016 3rd Conference on Control and Fault-Tolerant Systems (SysTol), IEEE, 2016, pp. 525–530.

[73] V. Subotić, M. Eibl, C. Hochenauer, Energy Conversion and Management 230 (2021) 113764. https://doi.org/10.1016/j.enconman.2020.113764.

[74] J. Milewski, K. Świrski, International Journal of Hydrogen Energy 34 (2009) 5546–5553. https://doi.org/10.1016/j.ijhydene.2009.04.068.

[75] K. Chaichana, Y. Patcharavorachot, B. Chutichai, D. Saebea, S. Assabumrungrat, A. Arpornwichanop, International Journal of Hydrogen Energy 37 (2012) 2498–2508. https://doi.org/10.1016/j.ijhydene.2011.10.051.

[76] M. Sorrentino, D. Marra, C. Pianese, M. Guida, F. Postiglione, K. Wang, A. Pohjoranta, Energy Procedia 45 (2014) 298–307. https://doi.org/10.1016/j.egypro.2014.01.032.

[77] M.A. Ansari, S.M.A. Rizvi, S. Khan, in: 2016 International Conference on Electrical, Electronics, and Optimization Techniques (ICEEOT), IEEE, 2016, pp. 4230–4234.

[78] D. Marra, M. Sorrentino, C. Pianese, B. Iwanschitz, Journal of Power Sources 241 (2013) 320–329. https://doi.org/10.1016/j.jpowsour.2013.04.114.

[79] M. Shao, X.-J. Zhu, H.-F. Cao, H.-F. Shen, Energy 67 (2014) 268–275. https://doi.org/10.1016/j.energy.2014.01.079.

[80] N.Y. Steiner, D. Candusso, D. Hissel, P. Moçoteguy, Mathematics and Computers in Simulation 81 (2010) 158–170. https://doi.org/10.1016/j.matcom.2010.02.006.

[81] C. Fischer, Anwendung statistischer Verfahren zur hydrologischen Modellierung in verschiedenen Thüringer Einzugsgebieten. Diploma thesis, Jena, 2008.

[82] C.E. Rasmussen, C.K.I. Williams, Gaussian processes for machine learning, MIT, Cambridge, Mass., London, 2006.

[83] M. Kuß, Gaussian process models for robust regression, classification, and reinforcement learning. Dissertation, Darmstadt, 2006.

[84] M. Ebden, Gaussian Processes: A Quick Introduction, 2015, http://arxiv.org/pdf/1505.02965v2, accessed 2021.

[85] O. Bousquet, U.v. Luxburg, G. Rätsch, Advanced lectures on machine learning: ML Summer Schools 2003 Canberra, Australia, February 2-14 2003 ; Tübingen, Germany, August 4-16 2003 revised lectures / Olivier Bousquet, Ulrike von Luxburg, Gunnar Rätsch, eds, Springer, Berlin, 2004.

[86] D. Duvenaud, Automatic Model Constructionwith Gaussian Processes. Dissertation, Cambridge, 2014.

Appendix

A. Derivation of correlation formula for *H/C* ≤ 4

With the definition of the *H/C*-ratio, the prerequisite that only alkanes are present as NG components and the structural formula of the alkanes, the following two equations (A.1) and (A.2) apply. The index “no” states that inert gas species are not considered.

$$\frac{H}{C}_{no} = \frac{K_{H,no}}{K_{C,no}} \tag{A.1}$$

$$K_{H,no} = 2K_{C,no} + 2 \tag{A.2}$$

Thus $K_{H,no}$ and $K_{C,no}$ if represented as a function of *H/C*-ratio

$$K_{C,no} = \frac{2}{\frac{H}{C}_{no} - 2} \tag{A.3}$$

$$K_{H,no} = \frac{2 \cdot \frac{H}{C}_{no}}{\frac{H}{C}_{no} - 2} \tag{A.4}$$

Using the definition of K_{e^-} in equation (10), $K_{e^-,no}$ is analytically calculated by substituting the equations of $K_{C,no}$ and $K_{H,no}$ into equation (A.5).

$$K_{e^-,no} = K_{H,no} + 4K_{C,no} = \frac{2 \cdot \frac{H}{C}_{no} + 8}{\frac{H}{C}_{no} - 2} \tag{A.5}$$

By the definition of K_H, K_C in equation (A.6) and (A.7) with respect to their values without inert gas species, the correlation between the real *H/C*-ratio of NG and the respective *H/C*-ratio without considering inert gas species is given by equation (A.8).

$$K_H = K_{H_{no}} \cdot (1 - x_{N_2} - x_{CO_2}) \tag{A.6}$$

$$K_C = K_{C_{no}} \cdot \left(1 - x_{N_2} - x_{CO_2}\right) + x_{CO_2} \tag{A.7}$$

$$\frac{H}{C}_{no} = \frac{2\frac{H}{C} \cdot (1-a)}{2 - a \cdot \frac{H}{C}} \quad , \quad a = \frac{x_{CO2}}{1 - x_{N_2} - x_{CO_2}} \tag{A.8}$$

Consequently, K_{e^-}, K_C and K_H is calculated according to equation (A.9) to (A.11).

$$K_{e^-} = \frac{2 \cdot \frac{H}{C}_{no} + 8}{\frac{H}{C}_{no} - 2} \cdot (1 - x_{N_2} - x_{CO_2}) \tag{A.9}$$

$$K_C = \frac{2}{\frac{H}{C}_{no} - 2} \cdot \left(1 - x_{N_2} - x_{CO_2}\right) + x_{CO_2} \tag{A.10}$$

$$K_H = \frac{2 \cdot \frac{H}{C}_{no}}{\frac{H}{C}_{no} - 2} \cdot (1 - x_{N_2} - x_{CO_2}) \tag{A.11}$$

B. Gaussian process regression

Machine learning algorithms are a common tool for estimation, regression and modelling and has been used in a variety of studies in general [69,70] and in the fuel cell field [71–80]. One of the best-known variants is the Gaussian process (GP). GP modelling is a supervised machine-learning algorithm based on known training data for model generation in classification and regression problems, where the latter is used in this work [69,81–83]. In-deep knowledge on GP modelling is found in Rasmussen [82].

GP has the following advantages for usage as regression model:

1. GP regression as non-parametric approach is not limited to a certain functional form to map input and output data, but rather needs only a mean and covariance function for its definition [69,82–84].
2. Noise from measurement errors can be incorporated in GP regression [82].

3. The estimated variance as part of the output of a GP regression captures the uncertainty of the estimation quantifiable [69].
4. In contrast to its complex theory, implementation is simple linear algebra [69].

A GP is defined by its mean function m(x) and its covariance function $k(x_i, x_j)$ for two input vectors x_i, x_j given in equation (B.1) and (B.2) [69,81–83,85]. A common assumption is zero as mean of the GP [81,82,84]. The covariance function or kernel defines a priori the covariance between functional values ($f(x_i), f(x_j)$) and contains the prior knowledge of a GP [69,81–84]. A typical covariance function is the squared exponential covariance function defined in equation (B.3), which is also called radial-basis function (RBF) [81–84,86]. Therein σ_f^2 is the signal variance (vertical scale) as maximum value of allowable covariance (for $x_i \approx x_j$) and l the characteristic lengthscale (horizontal scale) as hyperparameters, which need to be optimized [69,81,82,84,85]. The characteristic lengthscale l defines the distance of two correlated functional values describing the smoothness of the underlying function [69,82–84].

$$m(x) = E[f(x)] \tag{B.1}$$

$$k(x_i, x_j) = E\left[\left(f(x_i) - m(x_i)\right)\left(f(x_j) - m(x_j)\right)\right] \tag{B.2}$$

$$k(x_i, x_j) = \sigma_f^2 exp\left(-\frac{\|x_i - x_j\|^2}{2l^2}\right) \tag{B.3}$$

The functional values $f(x)$ for GP regression are said to be drawn of a multivariate GP, if they follow a joint Gaussian normal distribution as stated in equation (B.4) with mean function $m(x)$ and covariance function $k(x_i, x_j)$ for two input vectors x_i, x_j [69,81–84].

$$f(x) \sim GP\left(m(x), k(x_i, x_j)\right) \tag{B.4}$$

A new functional value f^* with the input vector x^* is estimated based on a GP model, which has been trained with known data [83]. Its output is a Gaussian distribution with its predicted mean μ^* as expected value for f^* at point x^* and a predicted variance of μ^*, which captures the uncertainty or confidence of the estimation [69,81,83–85].